Electronic supplementary materials *Mendeleev Commun.*, 2025, **35**, 746–748

The role of diglyme and tetraglyme in the formation of ion transport pathways in gel electrolytes based on polyethylene glycol diacrylate

Nikita A. Slesarenko, Alexander V. Chernyak, Vitaly I. Volkov, Kyunsilu G. Khatmullina, Alena V. Yudina, Galiya Z. Tulibaeva, Anna A. Slesarenko, Guzaliya R. Baymuratova, Alexander F. Shestakov and Olga V. Yarmolenko

Table of Contents

Experimental section

$LiBF_4$ (purity 98%) was used as electrolyte salt; bis(2-methoxyethyl) ether (diglyme, G2, purity >99%, 'Acros Organics'), tetraethylene glycol dimethyl ether (tetraglyme, G4, purity ≥99%, 'Sigma-Aldrich') was used as electrolyte solvent, and 1-ethyl-3-methylimidazolium tetrafluoroborate ($EMIBF_4$, Aldrich, purity ≥98%) was used as ionic liquid. Chemical reagents and diluents were acquired from Sigma-Aldrich and Acros Organics and used as received. Polyethylene glycol diacrylate (PEGDA, Aldrich, M_n = 700, mp 12–17 °C) was used to obtain a three-dimensional network matrix for the polymer gel electrolyte (PGE). The radical polymerization initiator, benzoyl peroxide (PB, Aldrich), stored in water (30%) was recrystallized from chloroform followed by drying at 20 °C in air and then *in vacuo*.

The structural formula of PEGDA is shown in Figure S1(*a*).

(*a*) (*b*)

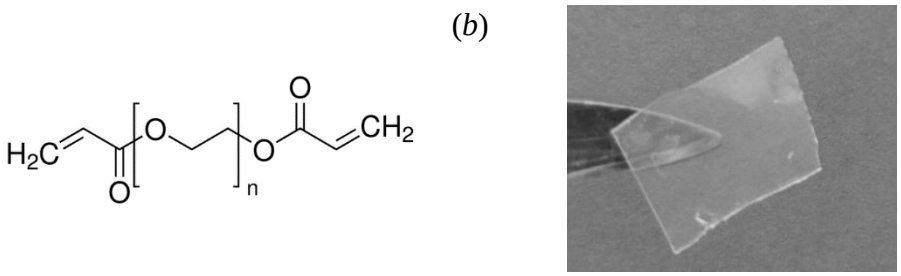

Figure S1 (*a*) Structural formula of PEGDA and (*b*) an optical photo of the PGE film.

The polymer electrolyte was synthesized by the radical polymerization of PEGDA in the presence of the radical initiator PB. The composition of the polymerizing mixture was as follows: PEGDA, $LiBF_4$, G2/G4, $EMIBF_4$ and 1 wt% PB for the entire sample. The curing of this mixture was carried out according to the following regime: 60 °C for 3 h, 70 °C for 1 h and 80 °C for 1 h.[S1] An optical photo of the final polymer electrolyte film is shown in Figure S1(*b*). It can be seen that the film is transparent.

To study the samples by NMR, PGEs were synthesized in closed glass capillaries of 4 mm diameter and 50 mm length. The capsules with PGEs were closed and placed in standard 5 mm diameter ampoules for NMR examination.

Analysis of PGE films by differential scanning calorimetry (DSC) was carried out in the temperature range from −100 to 20 °C on a Netzsch STA 449 F3 Jupiter thermal analyzer using Netzsch Proteus Analysis software at scanning speed 5 °C min^{-1}.

To measure the electrical conductivity of the PGE film samples by the electrochemical impedance method in symmetrical stainless steel (SS) cells SS//SS with an area of 0.2 cm^2, an Elins Z-2000 impedance meter (Chernogolovka, Russia) was used in the frequency range from 10 Hz to

600 kHz with a signal amplitude of 10 mV. The cell impedance was recorded in the temperature range from 0 to 60 °C. The measurement error did not exceed 2%.

To measure the resistance of the PGE/electrode interface at room temperature by the electrochemical impedance method in symmetric Li/Li cells, the Z-2000 impedance meter was similarly used. Symmetric cells with Li metal were assembled in coin-type CR2032 cells. The Nyqust plots of Li//Li cells were processed by the equivalent circuit method using the Zview2 program (https://www.scribner.com/software/68-generalelectrochemistr376-zview-for-windows).

Li-Battery Testing

The electrochemical performance of Li//$LiFePO_4$ (LFP) batteries was evaluated using a Neware Technology BTS-5 V 10 mA battery analyzer (Shenzhen, China) by performing charge/discharge cycles at a current density of 17 mA g^{-1} in the range of 2.6–3.8 V. The electrochemical performance of LFP was evaluated in coin-type CR2032 lithium batteries. The cathode composition included 75 wt% LFP, 20 wt% conductive carbon black (Timical Super C65) and 5 wt% PVDF polymer binder (Kynar Flex HSV 900, Arkema, Colombes, France). PGE was used as a separator. The boundary with the electrode was treated with 1 M LiTFSI in 1,3-dioxolane/dimethoxyethane (2:1) liquid electrolyte. The cells were assembled in an MBraun argon glovebox.

Diffusion coefficients were measured on a Bruker Avance-III 400 MHz NMR spectrometer equipped with a diff60 gradient unit (the maximum field gradient amplitude was 30 T m^{-1}) at temperatures from 0 to 60 °C. To measure the diffusion coefficients, PFG NMR was performed on ^{1}H (diffusion of solvent molecules and EMI^{+} ionic liquid cations), ^{7}Li (diffusion of lithium cations) and ^{19}F (diffusion of BF_4^- anions) nuclei at operating frequencies of 400, 155.5 and 376.5 MHz, respectively. A stimulated spin echo sequence was utilized. The experimental parameters of the NMR pulse sequences for ^{1}H, ^{7}Li and ^{19}F nuclei were as follows: $\pi/2$ pulses had durations of 9, 9 and 10 μs, gradient pulse durations δ were 1, 1 and 3.0 ms, and diffusion times Δ were 19.7, 19.7 and 49 ms, respectively. The repetition time was set to 3 s, and the magnetic field gradient was increased in 32 steps, reaching a maximum g value of 3.5, 11.5 and 4.0 T m^{-1} for ^{1}H, ^{7}Li and ^{19}F nuclei, respectively. The measurement error of the self-diffusion coefficients was 5%.

NMR relaxation method

The NMR relaxation times T_1 and T_2, as well as the line width of the NMR spectrum, are contingent on the modulation frequencies of local interactions, including magnetic dipole–dipole and quadrupole interactions. It is important to note that different relaxation times are sensitive to different frequency ranges of the fluctuation spectrum.[S2]

To interpret the relaxation measurements, it is necessary to employ a model of molecular motions. The simplest model used is thermal activation with an exponential correlation function. The spin–lattice relaxation rate is a function of the spectral density $J(\omega)$, the probability density of magnetic (electric) field fluctuations with a frequency close to the Larmor precession frequency is hereby represented. Assuming that the correlation time (τ_c) describes random motions of nuclei relative to their environment, the spectral density is calculated using the formula:

$$J(\omega) = \frac{\tau_c}{1+\omega^2\tau_c^2}\,. \tag{S1}$$

The spin–lattice relaxation rate for magnetic dipole–dipole interactions is defined as

$$\frac{1}{T_{1D}} = C_1\left[J\left(\omega_I\right)+J\left(2\omega_I\right)\right]+C_2\left[J\left(\omega_I-\omega_S\right)+3J\left(\omega_I\right)+6J\left(\omega_I+\omega_S\right)\right], \tag{S2}$$

where the first term of the equation describes the interactions between identical spins I–I, and the second term describes the interactions between different spins I–S, while the Larmor frequencies for nuclei I and S are denoted as ω_I and ω_S, respectively. The constants C_1 and C_2 are determined by the characteristics of the spin–spin interactions responsible for the relaxation.[S3,S4] For a nucleus with spin I = 1/2, the value of these constants determines the dipole–dipole homonuclear and heteronuclear interactions, which depend on the geometry of the structure and the number of interacting ^{7}Li nuclei. The phenomenon of NMR relaxation in PGE is primarily explained by two distinct mechanisms:

1) quadrupole relaxation $1/T_{1Q}$, as a result of the interaction of the quadrupole moment of the nucleus (eQ) with fluctuations in the electric field gradient caused by the charge distribution around the nucleus;
2) magnetic dipole–dipole relaxation $1/T_{1D}$, which is caused by random fluctuations of lithium nuclei and heteronuclear dipole–dipole interactions:

$$\frac{1}{T_1} = \frac{1}{T_{1D}} + \frac{1}{T_{1Q}}\,. \tag{S3}$$

For nuclei with spin $I > 1/2$, spin–lattice relaxation is determined mainly by quadrupole interactions:

$$\frac{1}{T_{1Q}} = C_Q\left[J(\omega_I)+J(2\omega_I)\right], \tag{S4}$$

where C_Q is the quadrupole interaction constant. This relaxation model, in accordance with expressions (S1) and (S2), predicts the minimum of the spin–lattice relaxation time T_1 (the maximum of the spin–lattice relaxation rate T_1^{-1}) under the condition $\omega\tau_c \approx 1$.

Table S1 Diffusion coefficients of slow and fast Li^+ cations [$D_s(^7Li)$] and their populations (I_1, I_2) measured using ^7Li nuclei at different temperatures, compared with diffusion coefficients [$D_s(^1H)$] of EMI^+ cations measured using ^1H nuclei.

T/°C	PGE1					PGE2				
	$D_s(^7Li)$				$D_s(^1H)$	$D_s(^7Li)$				$D_s(^1H)$
	I_1	Fast	I_2	Slow	EMI^+	I_1	Fast	I_2	Slow	EMI^+
0	0.20	1.0E-11	0.80	1.2E-12	9.3E-12	0.55	5.3E-12	0.45	3.7E-13	1.2E-11
10	0.13	1.7E-11	0.87	2.2E-12	1.1E-11	0.27	1.0E-11	0.73	8.4E-13	8.9E-12
22.5	0.10	2E-11	0.90	4.8E-12	1.7E-11	0.14	1.5E-11	0.86	1.9E-12	1.2E-11
30	0.08	2.8E-11	0.92	6.9E-12	2.4E-11	0.14	1.2E-11	0.86	2.8E-12	1.6E-11
40	0.06	4.6E-11	0.94	1.0E-11	3.4E-11	0.09	2.9E-11	0.91	4.5E-12	2.2E-11
50	0.13	3.7E-11	0.87	1.4E-11	4.9E-11	0.09	3.8E-11	0.91	6.9E-12	3.3E-11
60	0.09	6.1E-11	0.91	2.0E-11	6.3E-11	0.10	4.1E-11	0.90	9.7E-12	4.5E-11

Calculation of relative hydrodynamic radii R_{Li}

The calculations were carried out similarly to the published work.[S5]

From the Stokes–Einstein equation, the self-diffusion coefficient D can be determined as

$$\boldsymbol{D = \frac{kT}{c\pi\eta r_S}}, \quad \text{(S5)}$$

where c is a constant, η is the viscosity, and r_s is the Stokes radius for diffusing particles. Since the measurements of D of individual components are made for the same solution, the bulk viscosity should affect the diffusing particles in the same way. From $D_{ion} = \frac{kT}{c\pi\eta r_s^{ion}}$ and $D_{solv} = \frac{kT}{c\pi\eta r_s^{solv}}$ we can determine

$$\boldsymbol{R_{ion} = \frac{D_{solv}}{D_{ion}} = \frac{r_s^{ion}}{r_s^{solv}}}. \quad \text{(S6)}$$

The experimental value R_{ion} is a measure of the hydrodynamic size of the diffusing ion relative to the solvent.

Since the solvating medium for the polymer electrolyte was the ionic liquid $EMIBF_4$, which constituted 50 wt% and was 6 times greater in moles than the lithium cation and tetraglyme, and 3 times greater than diglyme, all calculations of the hydrodynamic radii of all ions and molecules R_X were carried out relative to the cation of the ionic liquid EMI^+ according to formula (S7):

$$\boldsymbol{R_x = \frac{D_{EMI+}}{D_X}}. \quad \text{(S7)}$$

Table S2 Results of calculation of relative hydrodynamic radius R_{Li}.

T/°C	PGE1			PGE2		
	Average	Fast	Slow	Average	Fast	Slow
0	3.00	0.92	8.01	--	2.24	32.16
10	2.65	0.66	4.89	2.56	0.85	10.48
22.5	2.61	0.86	3.60	2.92	0.81	6.38
30	2.77	0.84	3.44	3.45	1.34	5.50
40	2.62	0.74	3.29	3.15	0.77	4.86
50	2.66	1.31	3.41	3.25	0.85	4.75
60	2.62	1.03	3.15	3.43	1.09	4.60

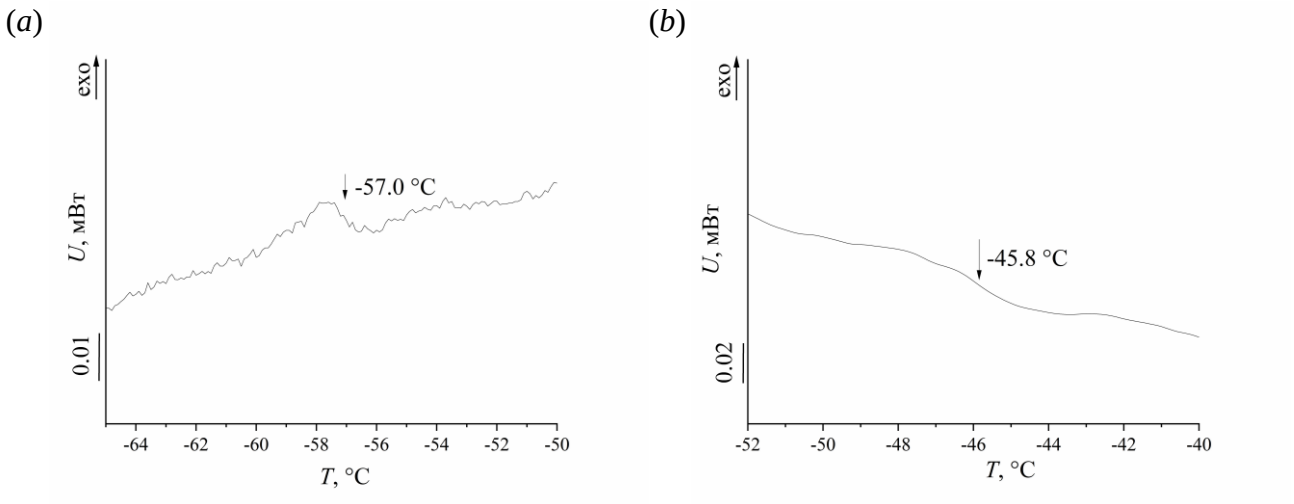

Figure S2 DSC curves of (*a*) PGE1 and (*b*) PGE2 in the temperature range where the relaxation transition of the polymer matrix occurs.

Quantum chemical modeling

Calculations were performed by the electron density functional method using the *ab initio* Perdew–Burke–Ernzerhof functional (PBE)[S6] and the extended basis set H [6s2p/2s1p], C, O [10s7p3d/3s2p1d], Li [10s7p3d/4s3p1d] for the valence shells. To model the structure of the polymer gel electrolyte (Figure S4), the effective Hamiltonian method was used taking into account the effects of van der Waals interactions.[S7]

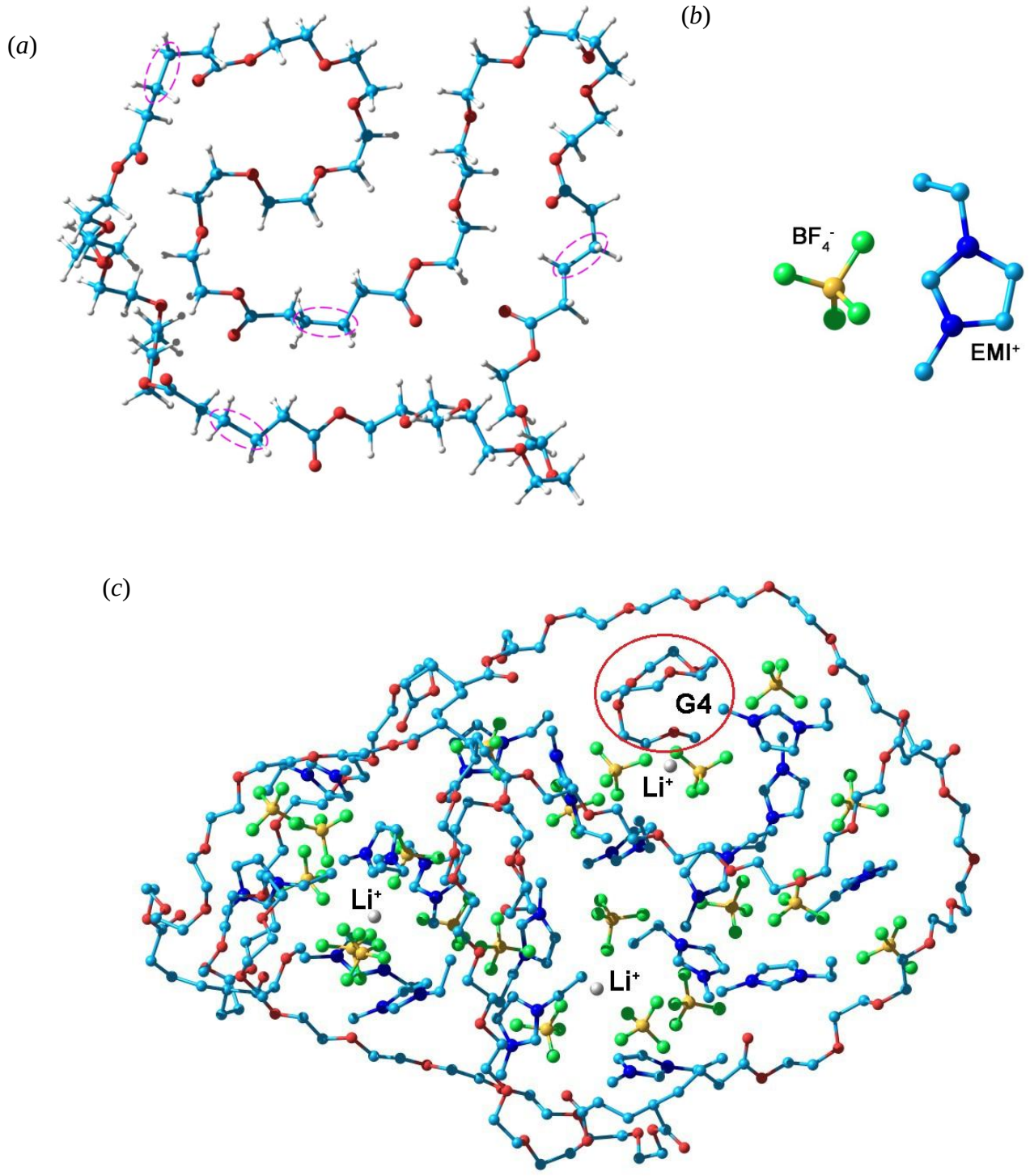

Figure S3 (*a*) Calculated structure of the simplest element of the polymer network consisting of 4 linked PEGDA fragments containing 6 (–CH_2CH_2O–) units. The dotted lines indicate the unit crosslinking sites, where the broken C–C bonds were replaced by C–H bonds. (*b*) Structure of the $EMIBF_4$ ionic liquid. (*c*) Structure of the polymer gel of the composition PEGDA–$LiBF_4$–$EMIBF_4$–G4 (1/1/6/1, mol/mol).

(*a*) (*b*)

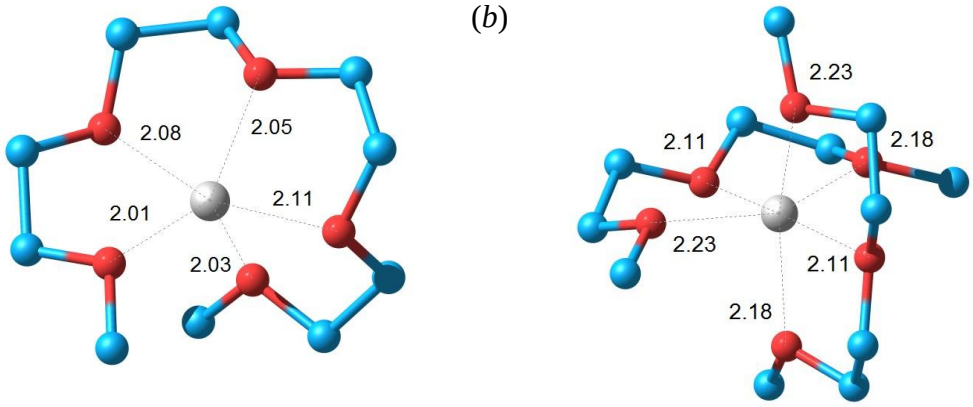

111.7 kcal mol^{-1} 120.3 kcal mol^{-1}

Figure S4 Solvate complexes (*a*) Li^{+}G4 and (*b*) $Li^{+}(G2)_2$ and their complexation energy.

Reaction	Energy	
PEG6 + $Li(G2)_2$ = PEG6(Li_G2) + G2	+0.3 kcal mol^{-1}	Figure S5(*d*)
PEG6 + $Li(G2)_2$ = PEG6(Li_G2a) + G2	−5.9 kcal mol^{-1}	Figure S5 (*e*)

(*a*)

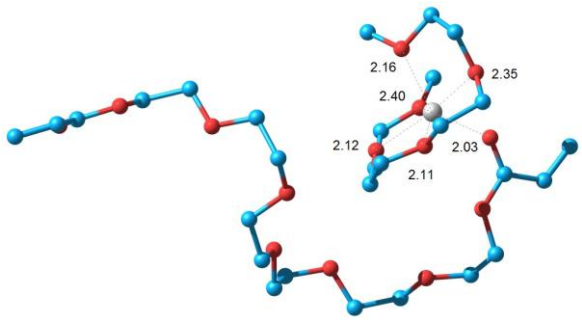

−19.0 kcal mol^{-1},ΔE_{total} = −130.7 kcal mol^{-1}

(*b*)

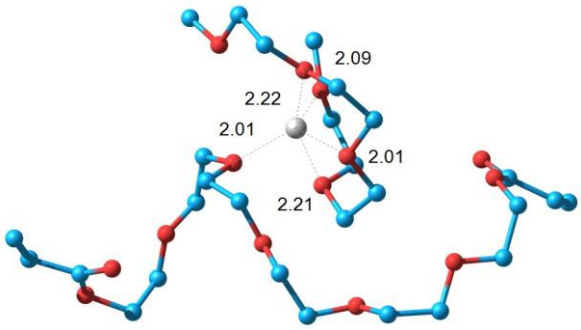

−17.4 kcal mol^{-1}, ΔE_{total} = −129.1 kcal mol^{-1}

(*c*)

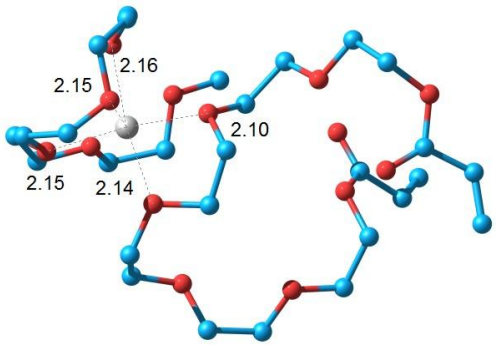

−17.2 kcal mol^{-1}, ΔE_{total} = −128.9 kcal mol^{-1}

(*d*)

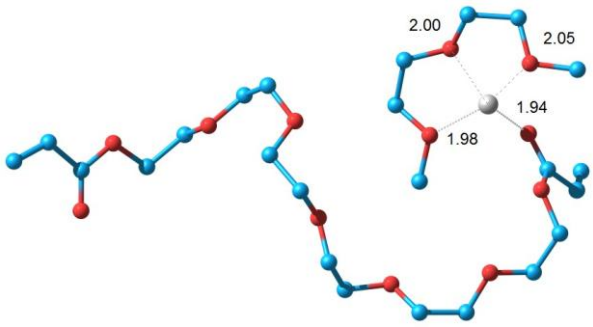

−35.8 kcal mol^{-1}, ΔE_{total} = −119.9 kcal mol^{-1}

(*e*)

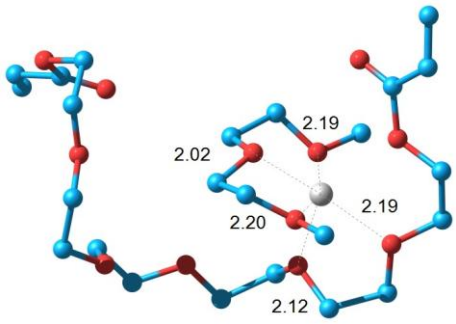

−42.0 kcal mol^{-1}, ΔE_{total} = −126.1 kcal mol^{-1}

Figure S5 Transport of solvate-shelled lithium cations, (*a*)–(*c*) Li^+(G4) and (*d*),(*e*) Li^+(G2), along the polymer chain with the lithium cation coordinated to the polymer chain *via* (*a*),(*d*) one carbonyl oxygen atom, (*b*) one ether oxygen atom or (*c*),(*e*) two ether oxygen atoms. Numbers indicate the binding energy of the lithium cation–glyme complex to the polymer chain.

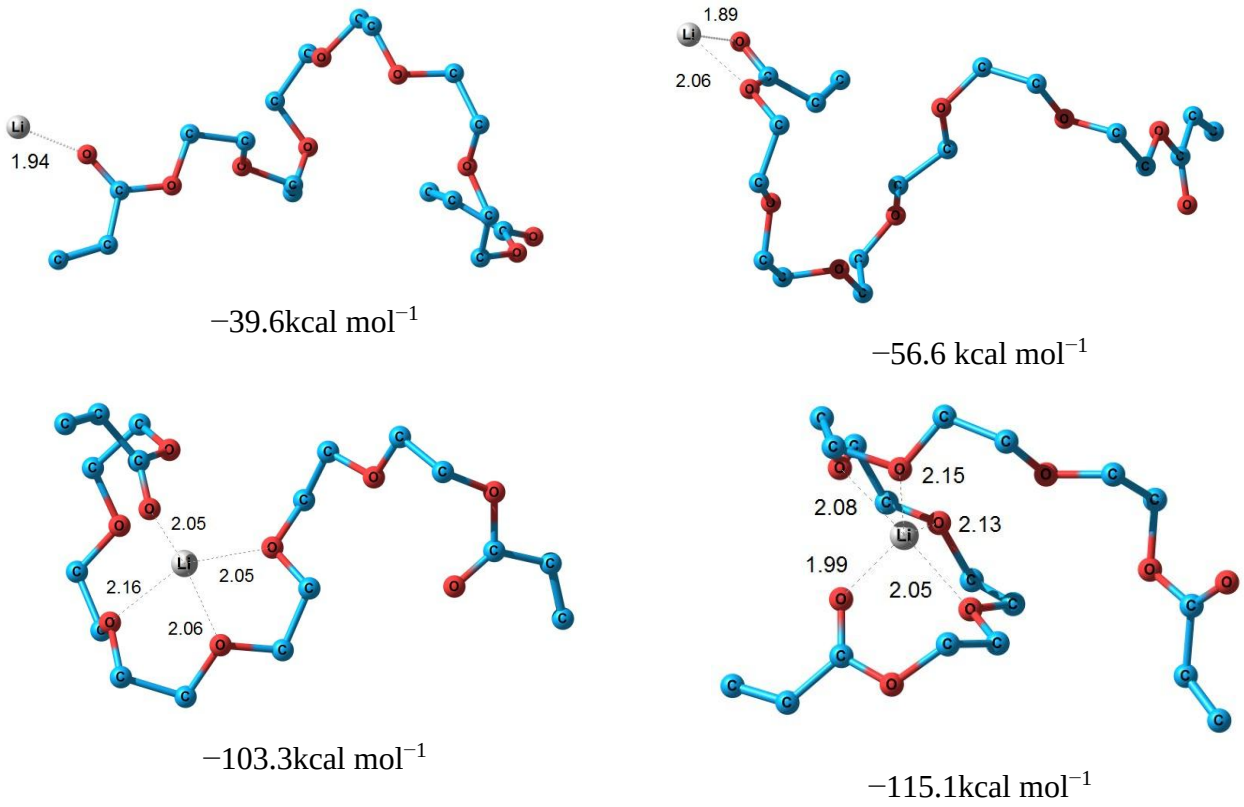

Figure S6 Transport of lithium cation along the polymer chain with the binding energy of lithium cation to the polymer chain indicated.

Table S3 Calculation of equivalent circuit parameters.

	PGE1			PGE2		
	1 day	2 day	3 day	1 day	2 day	3 day
R1, Ohm	11	17	19	10	20	22
R2, Ohm	47	177	212	23	280	359
R3, Ohm	344	784	717	202	871	960
CPE1-T, F	1.4×10^{-5}	1.4×10^{-5}	2×10^{-5}	1.4×10^{-5}	7.7×10^{-6}	9.7×10^{-6}
CPE1-P	0.76	0.74	0.72	0.8	0.75	0.74
CPE2-T, F	5×10^{-6}	6.35×10^{-6}	8×10^{-6}	6.6×10^{-6}	5.2×10^{-6}	6.2×10^{-6}
CPE2-P	0.87	0.87	0.87	0.87	0.87	0.88

(*a*)

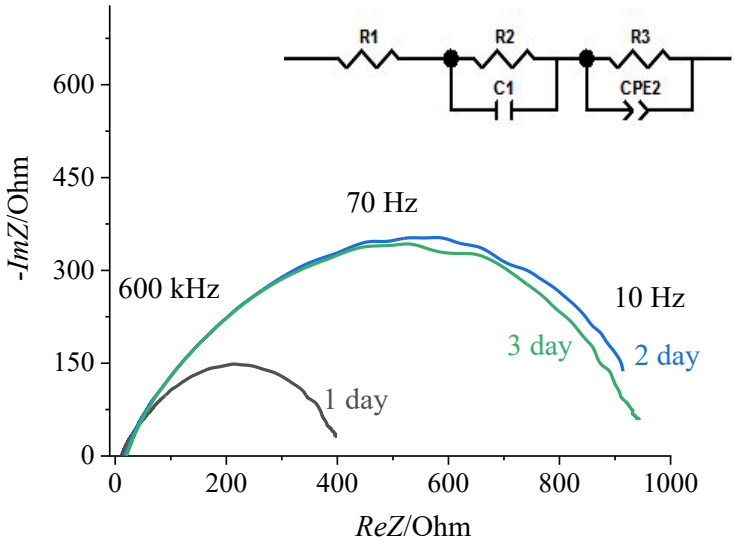

(*b*)

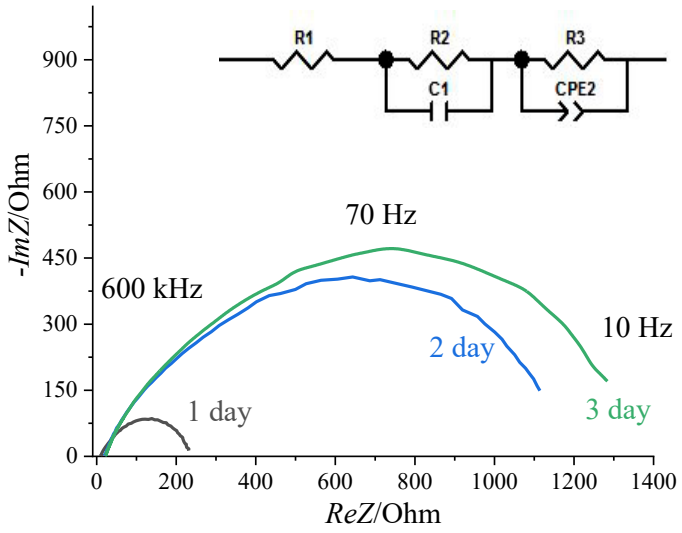

Figure S7 Nyquist plots of Li//Li cells with (*a*) PGE1 and (*b*) PGE2 and their equivalent circuits, where R1 is the PGE resistance, R2 is the SEI (solid electrolyte interface) resistance at the lithium surface, R3 is the charge transfer resistance, CPE1 is the SEI capacitance, and CPE2 is the double electrical layer capacitance.

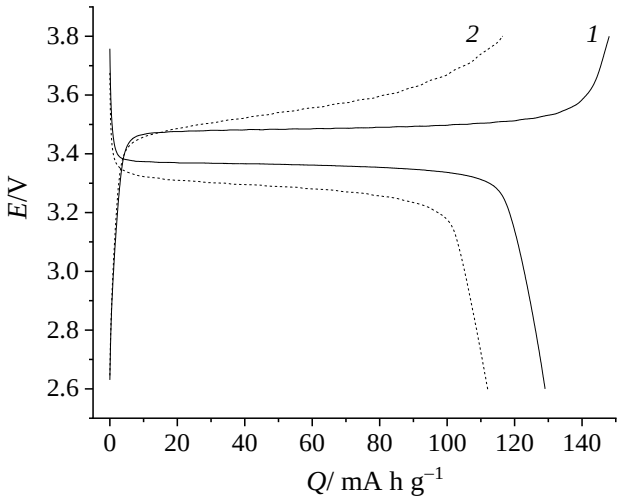

Figure S8 Charge–discharge profiles during cycle 10 for Li//$LiFePO_4$ cells with (*1*) PGE1 and (*2*) PGE2 at C/10 current in the range 2.6–3.8 V.

References

S1 A. V. Chernyak, M. P. Berezin, N. A. Slesarenko, V. A. Zabrodin, V. I. Volkov, A. V. Yudina, N. I. Shuvalova and O. V. Yarmolenko, *Russ. Chem. Bull.*, 2016, **65**, 2053; https://doi.org/10.1007/s11172-016-1551-4.

S2 A. Kessenikh, *Substantia*, 2021, **5**(2), 19; https://doi.org/10.36253/Substantia-1224.

S3 S. H. Chung, K. R. Jeffrey and J. R. Stevens, *J. Chem. Phys.*, 1991, **94**, 1803; https://doi.org/10.1063/1.459954.

S4 J. P. Donoso, T. J. Bonagamba, H. C. Panepucci, L. N. Oliveira, W. Gorecki, C. Berthier and M. Armand, *J. Chem. Phys.*, 1993, **98**, 10026; https://doi.org/10.1063/1.464435.

S5 K. Hayamizu and E. Akiba, *Electrochemistry*, 2003, **12**, 1052; https://doi.org/10.5796/electrochemistry.71.1052.

S6 P. Perdew, K. Burke and M. Ernzerhof, *Phys. Rev. Lett.*, 1996, **77**, 3865; https://doi.org/10.1103/PhysRevLett.77.3865.

S7 D. N. Laikov, *J. Chem. Phys.*, 2011, **135**(13), 134120; https://doi:10.1063/1.3646498.